U.S. DEPARTMENT OF ENERGY

PNNL-18334

Prepared for the
U.S. Nuclear Regulatory Commission
under a Related Services Agreement
with the U.S. Department of Energy
Contract DE-AC05-76RL01830

## Technical Letter Report

# Ultrasonic Flaw Detection of Intergranular Stress Corrosion Cracks as Observed In Austenitic Stainless Steel Piping Welds

## JCN N6398, Task 2A

S. L. Crawford
A. D. Cinson
M. T. Anderson
A. A. Diaz
S. E. Cumblidge

April 2009

Pacific Northwest
NATIONAL LABORATORY

## DISCLAIMER



PACIFIC NORTHWEST NATIONAL LABORATORY
*operated by*
BATTELLE
*for the*
UNITED STATES DEPARTMENT OF ENERGY
*under Contract DE-AC05-76RL01830*

PNNL-18334

**Technical Letter Report**

# Ultrasonic Flaw Detection of Intergranular Stress Corrosion Cracks as Observed In Austenitic Stainless Steel Piping Welds

**JCN N6398, Task 2A**

S. L. Crawford
A. D. Cinson
M. T. Anderson
A. A. Diaz
S. E. Cumblidge

April 2009

Prepared for
U.S. Nuclear Regulatory Commission
under a Related Services Agreement
with the U.S. Department of Energy
Contract DE-AC05-76RL01830

Pacific Northwest National Laboratory
Richland, Washington 99352

# Summary

The United States Nuclear Regulatory Commission (NRC) has sponsored Pacific Northwest National Laboratory (PNNL) to conduct a project titled "Reliability of Nondestructive Examination for Nuclear Power Plant Inservice Inspection." The objectives of the project are to (1) evaluate the accuracy and reliability of nondestructive examination (NDE) methods used for the inservice inspection (ISI) of nuclear power plant (NPP) systems and components; (2) provide information to the staff of the NRC to assess the adequacy of proposed industry changes to ISI programs; (3) provide recommendations to the staff of the NRC to improve the effectiveness and adequacy of ISI programs; (4) evaluate the effectiveness of ISI techniques in detecting cracks in reactor coolant system components (e.g., dissimilar metal welds, Alloy 52 weld overlays); and (5) provide technical assistance on NDE and related issues to the NRC program offices on an as-needed basis.

One of the major tasks is to address a wide range of NDE issues associated with coarse-grained steels and challenging material/component configurations, such as the far-side inspection on wrought stainless steel piping with austenitic welds in both boiling water reactor and pressurized water reactor configurations. PNNL conducted earlier ultrasonic studies on the far-side inspection in specimens containing implanted thermal fatigue cracks and machined notches. Results were favorable in that nearly all of the flaws were detected. This was followed by an ultrasonic phased-array (PA) inspection of specimens containing service-induced intergranular stress corrosion cracks (IGSCC) at the Electric Power Research Institute (EPRI) NDE Center, in Charlotte, NC, which is the subject of this report.

PA data were acquired on a series of specimens containing service-induced IGSCCs. True state information for all flaws was provided during the data analysis phase. The crack lengths were variable and PNNL only examined the specimens for circumferentially-oriented cracks (cracks that are parallel to the weld). Flaw depth information was not provided and flaw tip signals were not detected so no estimate of flaw depth was possible.

The investigation was focused on assessing current PA ultrasonic techniques for austenitic welds. Detection results should be considered as a best-effort, given equipment and inspection conditions; that is, the arrays were not specifically optimized for the weld conditions and the weld crowns were not removed, which would have provided greater access for each of the PA modalities and probes applied. Because the true state location data were known for the flaws under examination, the results described here should not be considered representative of a blind test, only an assessment of state-of-art phased array capabilities to detect actual service-induced IGSCC. Data were acquired with two refracted longitudinal wave PA probes, 1.5 MHz and 2 MHz, and one shear wave probe at 2 MHz from both the near and far side of the weld center relative to the flaw. The far-side detection rate for longitudinal mode inspections was nearly 70% while the detection rate for shear mode inspections was 52%. Signal-to-noise values for the detected flaws were good. Shear wave sound fields are believed to be significantly partitioned and attenuated (primarily by scattering) as they propagated through the austenitic weld material while the longitudinal wave sound fields generally maintain coherence with reduced scattering. Both shear and longitudinal data tended to be cluttered with geometrical and material reflections making signal discrimination the primary challenge in flaw detection. Suggested ways to improve the flaw detection include removing the weld crown for better access to the far-side region of interest and enabling probes with larger footprints; thus allowing large acoustic apertures for better sound field generation. The use of lower frequencies (longer wavelengths) may provide better penetration and reduce scattering effects, while more effective

approaches for peaking signals may improve signal discrimination. In addition, these suggestions, coupled with more accurate profiling of the complex part geometry in the critical area of examination, could collectively enhance the detection results from what is reported here.

# Acknowledgments

PNNL would like to thank several personnel at the EPRI NDE Center for enabling the work reported here. We appreciate Greg Selby's original invitation to collect and review IGSCC data on the practice specimens, and for making his staff available to PNNL during this activity. During the data collection and analyses, Carl Latiolais, Doug Kull, John Langevin, and Lief Esp provided their support to assist PNNL with set-up and true-state review. Mark Dennis facilitated the final contract to allow PNNL to review secure data. We also appreciate the comments provided by EPRI staff on the draft version of this report.

# Acronyms and Abbreviations

| | |
|---|---|
| ASME | American Society of Mechanical Engineers |
| BW | bandwidth |
| EPRI | Electric Power Research Institute |
| IGSCC | intergranular stress corrosion crack |
| ID | inner diameter |
| ISI | inservice inspection |
| LWR | light water reactor |
| NDE | nondestructive evaluation |
| NPP | nuclear power plant |
| NRC | Nuclear Regulatory Commission |
| NRR | Nuclear Reactor Regulation |
| OD | outer diameter |
| PA | phased array |
| PNNL | Pacific Northwest National Laboratory |
| SAFT | synthetic aperture focusing technique |
| SNR | signal-to-noise ratio |
| TRL | transmit-receive longitudinal |
| TRS | transmit-receive shear |
| $W_{cl}$ | weld centerline |

# Contents

# Figures



# Tables

# 1.0 Background

The United States Nuclear Regulatory Commission (NRC) has sponsored Pacific Northwest National Laboratory (PNNL) to conduct a project titled "Reliability of Nondestructive Examination for Nuclear Power Plant Inservice Inspection." The objectives of the project are to (1) evaluate the accuracy and reliability of nondestructive examination (NDE) methods used for the inservice inspection (ISI) of nuclear power plant (NPP) systems and components; (2) provide information for the staff of the NRC to assess the adequacy of proposed industry changes to ISI programs; (3) provide recommendations to the staff of the NRC to improve the effectiveness and adequacy of ISI programs; (4) evaluate the effectiveness of ISI techniques in detecting cracks in reactor coolant system components (e.g., dissimilar metal welds, Alloy 52 weld overlays); and (5) provide technical assistance on NDE and related issues to the NRC program offices on an as-needed basis.

The results obtained from this project will assist the NRC by supporting their technical reviews and will serve as confirmatory results for determining the effectiveness and adequacy of NDE and ISI methods and programs presently used in operating nuclear power plants. Recent experience with cracking in reactor vessel penetrations and piping welds has increased reliance on the ability of NDE methods to detect and characterize service-induced flaws over a range of materials, geometries, and configurations. The ability to detect and characterize flaws varies with the selected NDE method. With the industry trend toward reducing inspection time, radiation exposure, and the number of examinations, the effectiveness and reliability of NDE methods becomes more important.

Piping welds in the pressure boundary of light water reactors (LWRs) are subject to a volumetric examination based on Section XI of the American Society of Mechanical Engineers (ASME) Boiler and Pressure Vessel Code. Due to access limitations and a high background radiation, the technique used is primarily ultrasonic rather than radiographic. Many of the austenitic welds in safety-related piping systems have limited access to both sides of the weld so a far-side examination is necessary. Historically, far-side inspections have performed poorly because of the coarse and elongated grains within the microstructures of austenitic weld materials. The large grains cause the ultrasound to be scattered, attenuated, and redirected. Additionally, grain boundaries or weld geometry may reflect coherent ultrasound, making flaw detection and discrimination a more challenging endeavor.

Previous studies conducted at PNNL on ultrasonic far-side examinations in austenitic piping welds involved the application of conventional transducers, use of low-frequency Synthetic Aperture Focusing Techniques (SAFT), and ultrasonic phased array (PA) methods on specimens containing implanted thermal fatigue cracks and machined reflectors (Anderson et al. 2006; Anderson et al. 2007). From these studies, PA inspection provided the best results, detecting nearly all of the flaws from the far side. These results were presented at the Fifth International Conference on NDE in Relation to Structural Integrity for Nuclear and Pressurised Components in 2006. This led to an invitation to examine field-removed specimens containing service-induced intergranular stress corrosion cracks (IGSCC) at the Electric Power Research Institute (EPRI) NDE Center, in Charlotte, NC.

This report presents the work conducted by PNNL to acquire and analyze PA data on IGSCC specimens at the EPRI NDE Center to assess far-side examination methods. Section 2.0 describes the test specimens and Section 3.0 describes the PA inspection approach and associated probes and system. Results are presented in Section 4.0 followed by Section 5.0, which contains a summary and conclusions.

# 2.0 IGSCC Test Specimens

A number of specimens from the EPRI performance demonstration set were made available to PNNL for ultrasonic examination. These specimens were field-removed piping segments taken from several U.S. boiling water reactor primary re-circulation systems and contain service-induced IGSCC. Some of the specimens were part of a practice set and some were part of a secure set used for blind performance demonstration tests. PA data were acquired on both sets using identical techniques during a visit to EPRI in the fall of 2006. The practice data were taken back to PNNL for development of an analysis approach and the secure set was held at EPRI for subsequent data analyses.

## 2.1 EPRI Performance Demonstration Practice Specimens

A number of welded specimens containing service-induced intergranular stress corrosion cracks were available for examination at the EPRI NDE Center. These specimens varied in configuration with different weld crown geometries, counterbore, weld root conditions, etc. Figure 2.1 and Figure 2.2 show some of the variation in specimens as viewed from the outside and inside of the pipe segments. Specimens had a nominal 28-in. (71-cm) diameter and 0.8–1.6-in. (2.0–4.1-cm) wall thickness. A mapping of the flaws was provided, showing flaw location in the circumferential direction and axial position as upstream or downstream from a weld center line ($W_{cl}$). However a $W_{cl}$ was not marked on the specimen so axial position for acquired data was referenced relative to the center of the weld crown. True-state location and length sizing information was given but no true state depth information was available. The examinations for this activity focused on detection of ID-connected cracks, oriented circumferentially (parallel to the weld).

**Figure 2.1**. Examples of Specimens as Viewed from the Outer Surface

**Figure 2.2**. Examples of Specimens as Viewed from the Inner Surface

## 2.2 EPRI Performance Demonstration Secure Specimens

The secure specimens were similar to the practice specimens but access was limited to the outer surface only. These specimens are used by EPRI in administering performance demonstration evaluations so the specimen number and flaw information are purposefully not revealed to maintain the integrity of the test set. The flaw true state was provided to PNNL personnel during proctored data analysis activities at the EPRI NDE Center and the secure true state information was not allowed to leave the testing room.

# 3.0 Phased-Array Inspection

The PNNL PA system used for data acquisition consisted of a Tomoscan III® 32-channel instrument, available off-the-shelf from ZETEC, Inc. The instrument can be programmed by the development of focal laws to control up to 32 channels for transmission and reception of ultrasonic signals. It incorporates 12-bit logic and operates through a local Ethernet connection to a standard desktop computer.

## 3.1 Phased-Array Probes

The basic premise for all PA transducers involves a set of small, individual piezoelectric elements that are independently driven. Although these elements may be pulsed individually, or in groups, to

simulate conventional transducer excitation, the real strength of this technique lies in the capability of the system to electronically delay each of these elements during both generation and reception of ultrasonic sound fields. The wave-fronts produced by subsets of elements interfere within the inspected component to produce a resultant, phase-integrated ultrasonic wave; this process is commonly referred to as *beam forming*. The PA system can therefore steer and focus the integrated ultrasonic beam within the component. This allows a single array to inspect a component with variable inspection angles and focusing depths almost simultaneously. Theoretically, an entire pipe weld can then be examined with a single circumferential scan motion.

Three PA probes were used in this work and included two transmit-receive longitudinal (TRL) wave probes, one designed to operate at 1.5 MHz and one at 2 MHz, and a 2-MHz transmit-receive shear (TRS) wave probe. All three probes were specially designed for near- and far-side applications in austenitic material ranging from approximately 0.5 to 1.5 in. (13 to 38 mm) in thickness. The 2-MHz probes, shown in Figure 3.1, were used in the earlier PNNL far-side study (Anderson et al. 2006; Anderson et al. 2007) on thermal fatigue cracks and machined flaws. These two probes have integral wedges that were contoured to fit the appropriate pipe curvature for these specimens. The 1.5-MHz probe is depicted later in Figure 3.6 and was designed specifically for the far-side IGSCC inspection. It contains three elements in the secondary direction which allows for improved lateral (side-to-side) beam skewing.


**Figure 3.1**. Integral Wedge Design 2-MHz TRL Probe (left) and 2-MHz TRS Probe (right)

The 2 MHz TRL array was designed for near- and far-side applications in thinner pipe sections. It consists of two, 2-element by 14-element, matrix arrays. One array is used for transmitting, the other for receiving ultrasonic signals. The highly damped probe has a 70% bandwidth (BW) at -6 dB and an approximately 25-mm$^2$ footprint with an integral wedge for data collection in tight geometrical configurations. This smaller size generally allows insonification of the far side even with a weld crown present. The probe's nominal wavelength in stainless steel is 3.0 mm at its average center frequency of 1.9 MHz. Skew angles of ±10 degrees were possible with this array.

The 1.5-MHz TRL array consists of two, 3-element by 10-element, matrix arrays with a 62% bandwidth at -6 dB. This array is designed with a non-integral wedge allowing change out of the wedge for inspecting pipes of varying diameters or flat plates. Its footprint is approximately 50 by 50 mm. The larger size and increased number of elements in the lateral direction provides improved beam forming and

skewing but limits its application in tight geometrical conditions. This TRL array has a wavelength of 3.8 mm in stainless steel, at its average center frequency of 1.5 MHz. Skew angles of ±10 and ±20 degrees were possible with the larger number of elements in the secondary axis of this probe.

The 2-MHz TRS array consists of two, 24-element linear arrays with an integral wedge. Its footprint is approximately 50 by 30 mm. The array has a -6 dB bandwidth of 65% and an average wavelength of 1.4 mm in stainless steel at its center frequency of 2.14 MHz. Skewing was not possible with this array.

Focal laws were developed for the TRL and TRS arrays and programmed into the UltraVision® acquisition software. The focal laws were developed to provide ultrasonic longitudinal beam angles from 30° to 70° at 1° increments for the 2.0-MHz TRL array in the piping specimens, and from 40° to 70° at 1° increments for the 1.5-MHz TRL. Shear wave focal laws were developed for the 2.0-MHz TRS array to provide beam angles from 40° to 70° at 1° increments. This resulted in the sound field being swept through many discrete beam angles in near real time at each position along the entire length of the linear scan. In other words, for each axially oriented cross section of material, data were acquired from 30° to 70° or from 40° to 70°, while the linear scans progressed circumferentially.

Sound field modeling results are summarized in Figure 3.2 through Figure 3.4 for the 1.5-MHz TRL, 2-MHz TRL, and 2-MHz TRS probes in stainless steel. The left portion of each figure shows an idealized sound field as a function of depth, in a side view, for a 45° inspection angle. The designed focal depth is noted in the image by a black crossed circle. A top view of the sound field at the focal depth is shown in the right portion of each figure. Note that the top view color scheme has been normalized to show the full color range, white to red, in the view. Reference lines separated by 2 mm are displayed in Figure 3.2 through Figure 3.4 to show scale. Theoretical spot sizes as measured from these simulations at the red level, approximately 3 dB points, are 3.4 by 2.7 mm for the 1.5-MHz TRL probe, 5.0 by 4.3 mm for the 2-MHz TRL probe, and 2.9 by 1.7 mm for the 2-MHz TRS probe. The spot sizes at the yellow, approximately 6 dB points, are 9 by 6.9 mm for the 1.5-MHz TRL probe, 11.2 by 9.0 mm for the 2-MHz TRL probe, and 7.2 by 2.6 mm for the 2-MHz TRS probe.

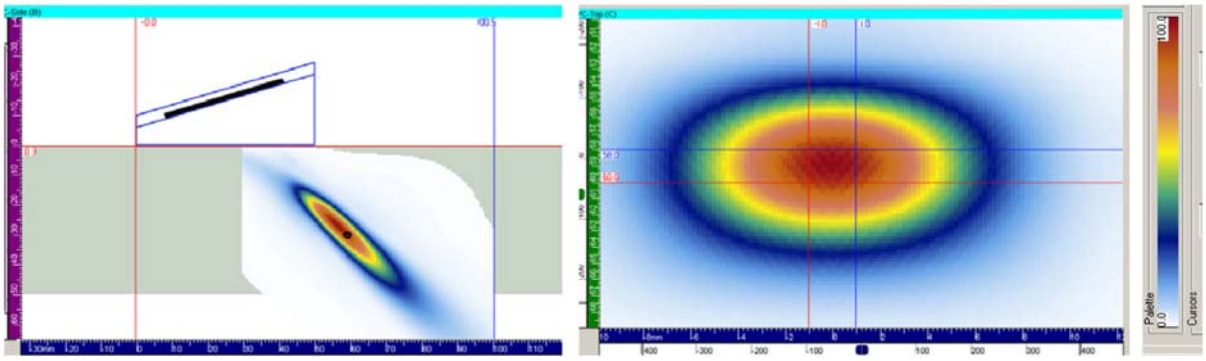

**Figure 3.2**. TRL 1.5-MHz Beam Model at 45° with the Side View on the Left and Top View on the Right. The top view is at the focal depth of 30 mm. Vertical and horizontal lines with 2-mm separation are shown for reference.

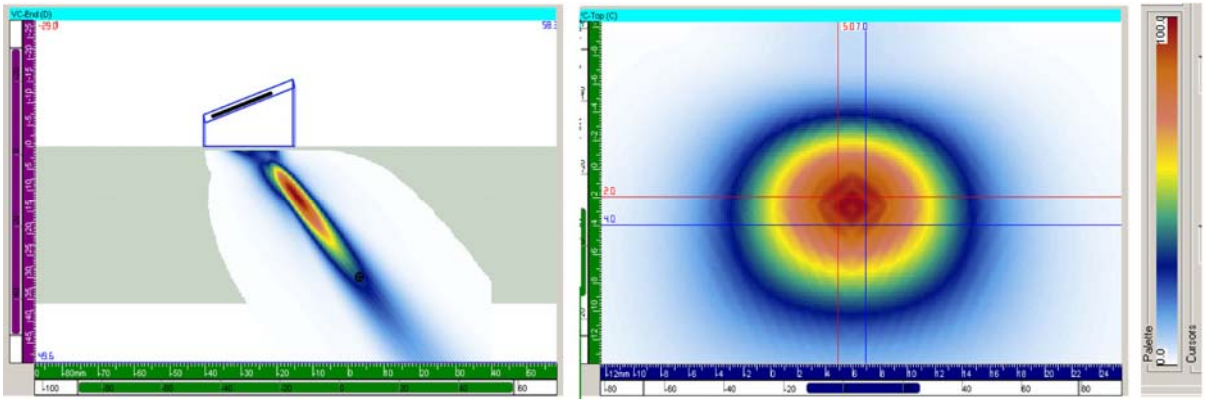

**Figure 3.3**. TRL 2-MHz Beam Model at 45° with the Side View on the Left and Top View on the Right. The top view is at the focal depth of 30 mm. Vertical and horizontal lines with 2-mm separation are shown for reference.

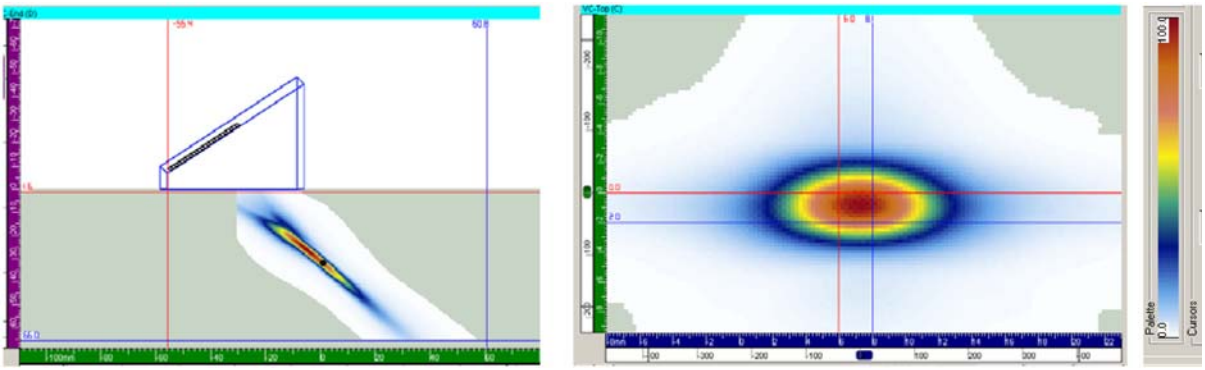

**Figure 3.4**. TRS 2-MHz Beam Model at 45° with the Side View on the Left and Top View on the Right. The top view is at the focal depth of 32 mm. Vertical and horizontal lines with 2-mm separation are shown for reference.

These beam plot images show that the 1.5-MHz TRL and 2-MHz TRS arrays are operating near the center of their focal region at a depth of approximately 30 mm. At this depth the 2-MHz TRL array is performing beyond its ideal focal plane as shown in the side view of the beam plot in Figure 3.3; however, in practice, good signals at the 30-mm depth were detected and recorded. The advantage of this 2-MHz TRL probe is its small footprint which allows better sound field access to the far side of the weld in the presence of a limiting weld crown or other geometrical condition. On at least one of the EPRI pipe specimens this was the only probe that could effectively collect data on both sides of the weld due to geometrical constraints.

Additional beam field modeling for the 1.5-MHz TRL array shows the ability of the probe to form a coherent beam at skew angles up to 20°. The modeling results are shown in Figure 3.5. Skewed data can improve detection of IGSCC because it can be more sensitive to cracks branching out of the primary plane of the flaw and also be less sensitive to planar geometrical reflectors such as counterbore.

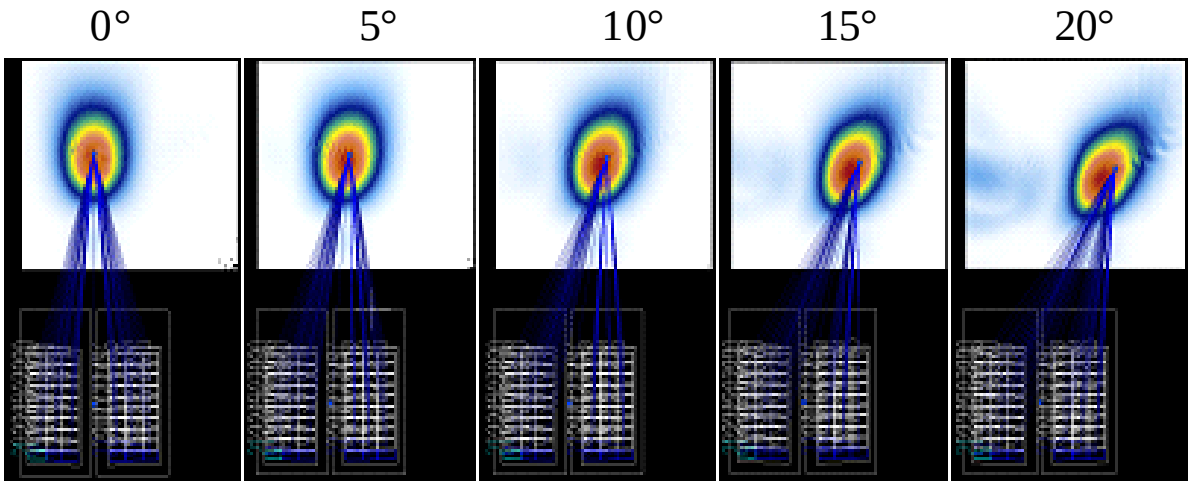


**Figure 3.5**. Beam Skewing Model for the 1.5-MHz TRL, 10 by 3 Element Probe

## 3.2 Scan Protocol

For the three probes and all specimens, data were acquired with a manual scanner. The scanner was mounted on a curved section or ring positioned adjacent to the specimen. The 1.5-MHz TRL probe and scanner are shown in Figure 3.6. Data were acquired with the sound beam directed perpendicular to and pointing toward the weld, while the manual scanner was moved in the circumferential direction. The scanner encoder was calibrated to the specimen to give circumferential positional information. Several linear scans were acquired from both the near side and the far side when specimen configuration allowed. A line scan with the probe positioned as close as possible to the weld crown center was acquired first. Additional scans with added offsets from this first position were then acquired from both sides when possible, typically at offset distances of 0.25 in. (0.64 cm) and/or 0.5 in. (1.27 cm). The line scans proceeded clockwise with respect to the flow and the flow direction was noted by an arrow on the specimens. Skewed data were also acquired because the flaws were service-induced IGSCCs and typically exhibited branching out of the plane of the flaw parallel or axial to the weld. Data obtained at skewed angles can be sensitive to the crack branching, and when combined with the normal data, may improve the flaw detection. Skew angles of ±10° and ±20° were used with the 1.5-MHz TRL probe. The linear TRS probe was not skewed and the 2.0-MHz TRL probe was skewed at ±10°. Data were acquired such that each file contained only a single skew angle. The default skew was 0°.

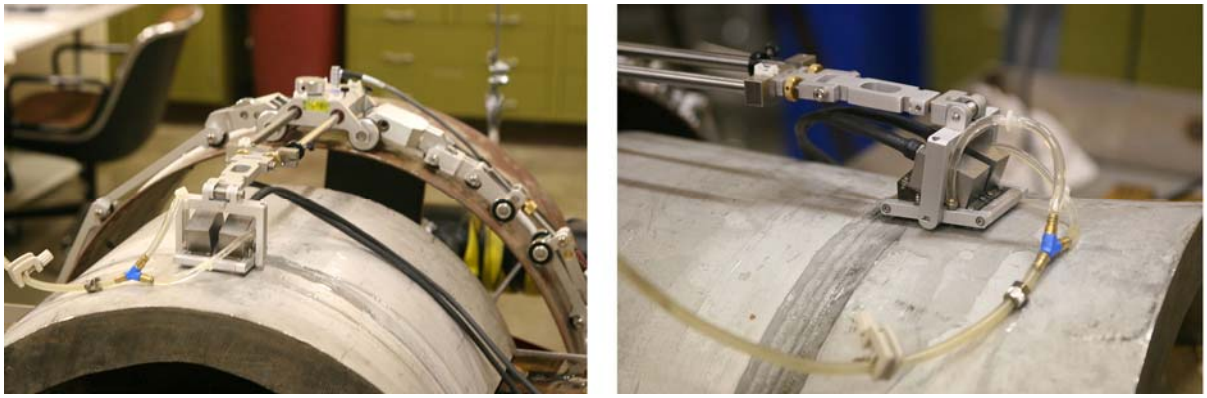

**Figure 3.6**. Mechanical Scanner Mounted on a Ring Section in the Background with the Scanner Arm and Probe Extending to the Foreground (left) and Side View of the 1.5-MHz TRL Probe Next to a Weld (right)

# 4.0 Phased-Array Results

## 4.1 Detection

Flaw data from the EPRI specimens were analyzed for detection with the three PA probes. The detection criteria are discussed here. Given the true state of a specimen, if a clear response that was distinct from geometry and possessing a good signal-to-noise ratio (SNR) was found at any of the skew angles in the region noted as flawed, a "Yes" result was recorded for the flaw. If a weak signal that was discernable but not clearly separate from geometry or close to the noise levels was found in the region noted as flawed, a "Marginal" result was recorded. If no signal was found in the region noted as flawed, then a "No" result was recorded.

Figure 4.1 shows data from a region classified as "Yes" in the detection results. Arrows point to the flaw signals in the three views. The top view shows an ID geometrical signal on the left edge that runs nearly the entire length of the scan. The flaw signal is farthest to the right in the top view with other material reflectors in the middle. The signal of interest is gated in the side view using red and blue vertical lines and these gated results are shown in the end view. Arrows in the end view point to the flaw.

Figure 4.2 shows data from a region that was categorized as "Marginal" in detection. There is a signal in the region of interest that is slightly higher than the background but it does not have much length associated with it compared to surrounding area signals. Another signal in the data (end view) with similar amplitude stands out as a possible flaw but this region was not shown to be flawed. This could potentially lead to a false call in this area. False calls were not tracked in this analysis but contributed to the Marginal result as opposed to Yes detected calls.

Figure 4.3 shows data from a region that was classified as "No" in detection. There is no signal in the flaw region that stands out from the surrounding area. A lack of signal might be evident in the region of interest in the end view but this was not used as one of the flaw criteria.

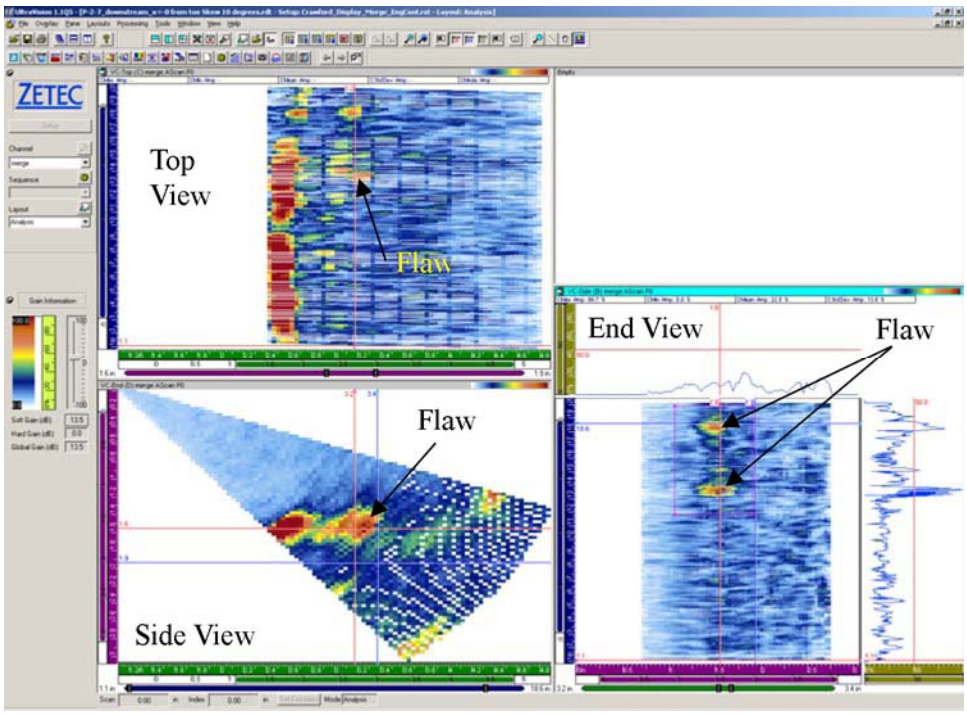


**Figure 4.1**. Example of a "Yes" Call

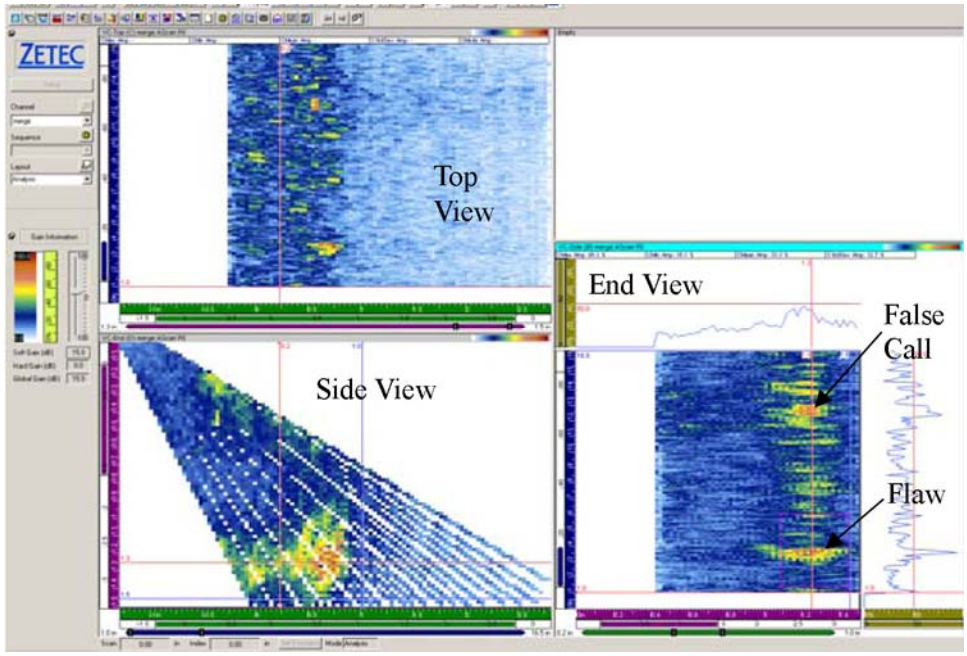


**Figure 4.2**. Example of a "Marginal" Call

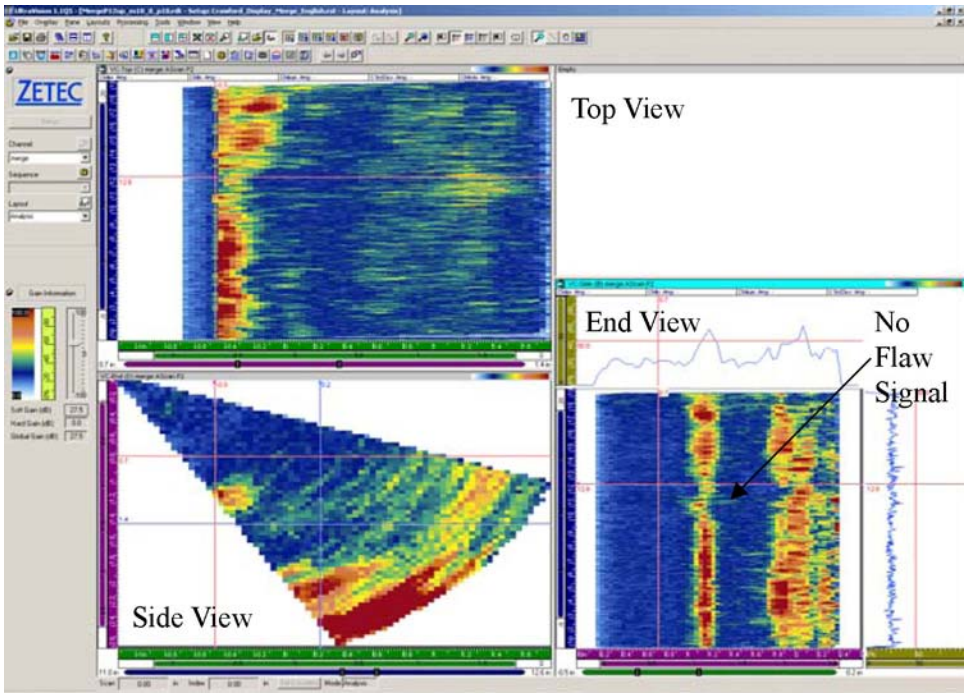


**Figure 4.3**. Example of a "No" Call

## 4.2 Results

The practice data were taken to PNNL and analyzed shortly after the data acquisition trip. Some of the images and detection calls are shown in Appendix A from both the near and far side. The data are presented from the downstream side first for a given specimen and then from the upstream side for the three PA probes. The secure data were then later analyzed at the EPRI site. Data images and information on detection calls relative to particular specimens were not allowed to leave the EPRI testing room. Only approved summary information is included in this report. The results from the two separate sets of data are shown in Figure 4.4. The "Yes" calls are represented with blue boxes, the "Marginal" calls with green triangles, and the "No" calls with brown circles. Secure data are shown with dotted line connections and the practice data with solid lines. Results for the three probes from the near side and far side are provided. In most of the data sets, the far-side "Yes" call is lower than the near side "Yes" call, as expected. However from the secure set at 1.5-MHz TRL, the near side and far side "Yes" detected calls are the same at approximately 80%. Differences in results from the secure and practice data sets are likely due to experience of the data analysts in interpretation or in the specimens themselves. In general, the Yes calls fall in the 50% to 80% range for the far-side inspection.

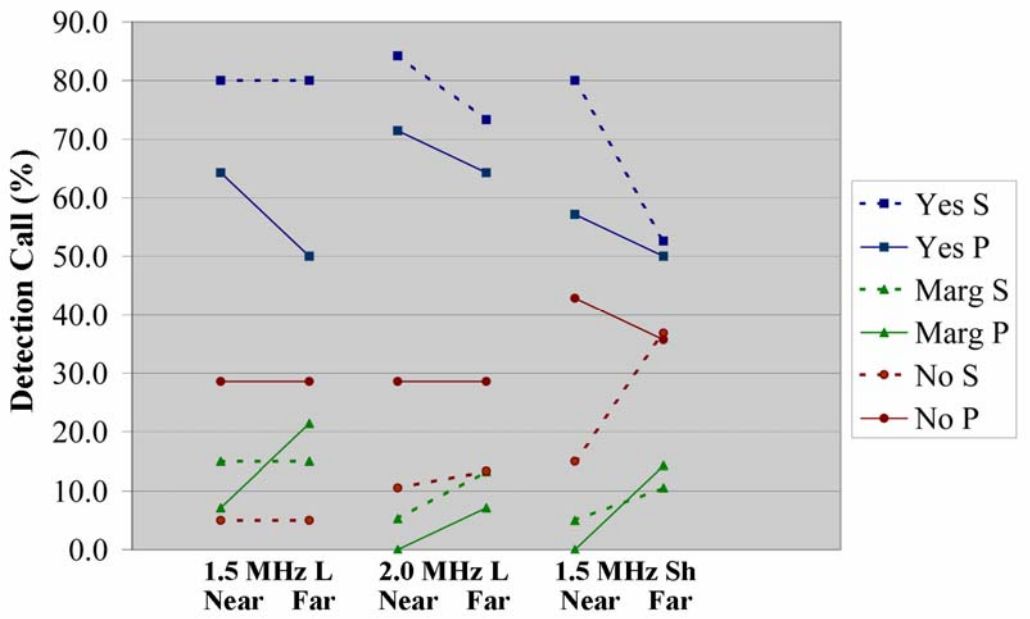


**Figure 4.4**. Detection Calls on the Secure and Practice Data Sets as a Function of PA Probe and Near- and Far-Side Inspection

The secure and practice data results were combined to give a larger sample population and to protect the integrity of the secure set. A summary of the results are listed in Table 4.1. This combined data set represents a number of service-induced cracks in a variety of pipe and component configurations joined with an austenitic weld. The depth of the cracks were not known nor measured from the data as tip-diffracted signals were not sought out. The lengths of the cracks were variable, as reported by EPRI true state information. This study focused on flaw detection, so crack lengths were not measured. In general, cracks on the small end of the observed length range could be confused with material noise, and cracks on the long end of the range could be confused with part geometrical reflectors such as counterbore or weld root. Medium to long indications whether from a flaw or geometry could also exhibit signal drop out due to sound field redirection, scattering, or attenuation. These issues make signal discrimination more challenging.

**Table 4.1**. IGSCC Detection Summary

| | 1.5-MHz TRL | | | 2.0-MHz TRL | | | 2.0-MHz TRS | | |
|---|---|---|---|---|---|---|---|---|---|
| **Access** | **Yes** | **No** | **Marginal** | **Yes** | **No** | **Marginal** | **Yes** | **No** | **Marginal** |
| Near Side | 73.5 | 14.7 | 11.8 | 78.8 | 18.2 | 3.0 | 70.6 | 26.5 | 2.9 |
| Far Side | 67.6 | 14.7 | 17.6 | 69.0 | 20.7 | 10.3 | 51.5 | 36.4 | 12.1 |

The detection summary shows that a near-side inspection using methods similar to those described in this report will be superior with approximately 70% to 80% of the flaws being detected. On a far-side inspection using similar methods, the detection rate drops to approximately 50% for shear waves and is just under 70% for the longitudinal wave modality.

Flaw detection generally involves two parts. One part of the detection process relates to signal amplitude. How high above the background noise level is the signal of interest? A measurement used for this process is the SNR. An SNR of at least two to one, or 6 dB, is commonly desired, but current analytical techniques allow lower values with most procedures requiring analyses of flaw responses down to the material noise level. The SNR for these data were calculated from the peak signal responses from "Yes" detected flaw responses and the average noise level around the flaws. Noise values were taken at the same part path as the signal responses. SNR values from the different detected cracks were averaged with results shown in Figure 4.5 for each probe and for near- and far-side access. Results indicate that the SNR values are good; all exceeding 10 dB (signal is 3.2 times the noise level). The higher near-side SNR for the TRS probe is possibly due to the lack of mode conversion taking place. From the far side, the SNRs are similar for each of the three probes for a detected flaw. With SNRs being adequate in these data sets, the challenge in flaw detection then becomes one of signal discrimination.

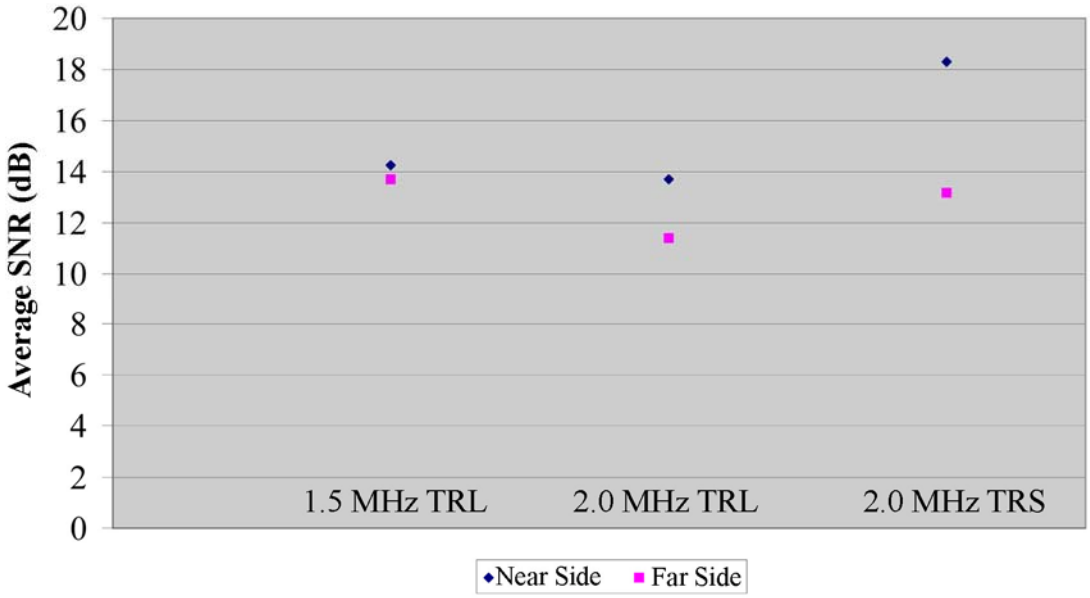


**Figure 4.5**. Signal-to-Noise Ratios for "Yes" Detected Cracks

Another major step for flaw detection is in signal discrimination—is the ultrasonic response being generated from a geometrical condition, material noise, or a flaw? Ideally, one would determine the weld area profile along the pipe axis using a contour gauge on the OD surface and UT thickness readings to exhibit the approximate ID contour. These contour measurements were not made during this exercise. In addition, the presence of weld crowns would prohibit the collection of a normal (0-degree) beam ultrasonic measurement to map the ID weld region. If the weld area is diagramed, indications from subsequent specimen evaluations can be mapped to the originating location in the specimen profile. Signals mapped to the counter bore, weld root, etc. may then be classified as geometrical indications. Often geometrical signals have significant length and amplitude associated with them. A strong counterbore signal provides a reference point for all other signals whether the weld area profile is known or not. As an example of a known configuration, an austenitic stainless steel piping specimen typical of that found in a primary coolant BWR recirculation system, was fabricated with sawcuts and implanted

thermal fatigue cracks. The weld cross section is shown in Figure 4.6. PA data acquired from the far side of the flaw is shown in Figure 4.7. The sector side view on the left of Figure 4.7 shows, from left to right in the image, a geometrical signal from the inner diameter mismatch step, a geometrical signal from the weld root, and the flaw signal.

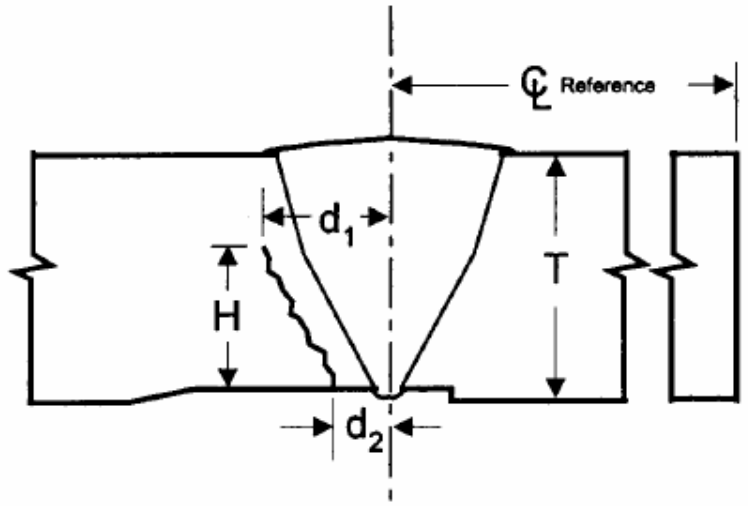


**Figure 4.6**. Cross-Sectional Schematic Showing the Weld Geometry and Location of an Implanted Crack in the Weld Heat Affected Zone

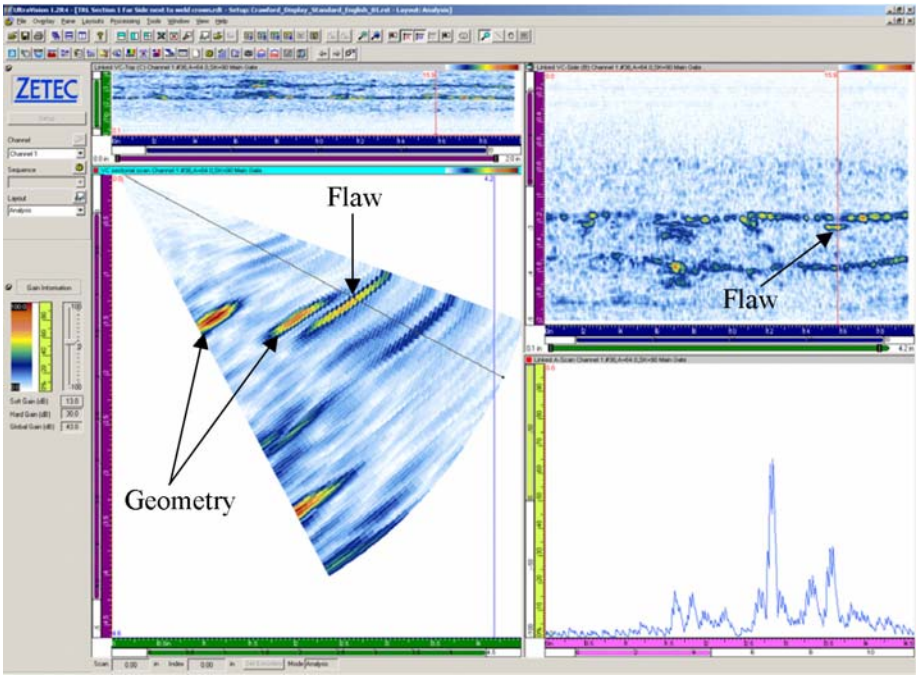


**Figure 4.7**. Far Side Data from a Specimen with the Cross-Section Shown in Figure 4.6. Geometrical signals from the inner diameter mismatch step and weld root are noted. The flaw signal is also identified.

Data from the EPRI specimens were generally not as straight forward and were cluttered with many signals to consider. Figure 4.8 shows near side data from a practice specimen. The geometrical signal from the far side of the weld is clearly seen and can be used as a reference. The side view shows three main reflectors between the red and blue horizontal lines. This region is gated and shown in the top view. The far-side geometrical signal is identified and all other signals referenced to it. Notice that the far-side geometry produces a strong signal, but with signal dropout evident. The flaw signal is sandwiched between two geometrical signals in the side and top views and the near-side geometry signal does not extend the full length of the image. The vertical red and blue lines in the side view are used to gate out the flaw signal with results shown in the end view. The flaw signal is at the bottom of the end view and is boxed with the magenta lines. Other signals are detected at that same axial position but are lower in amplitude. For this reason, the flaw was considered "Yes" detected. In general, for data analyses, a narrow vertical gate such as that shown in the side view is moved across the image while looking at the end view for signals of interest. In the PNNL analyses, one considered if there was a signal in the area noted as flawed that was separable from other signals and of higher amplitude. All images in this report are from merged data but unmerged data were also reviewed during the flaw detection analyses.

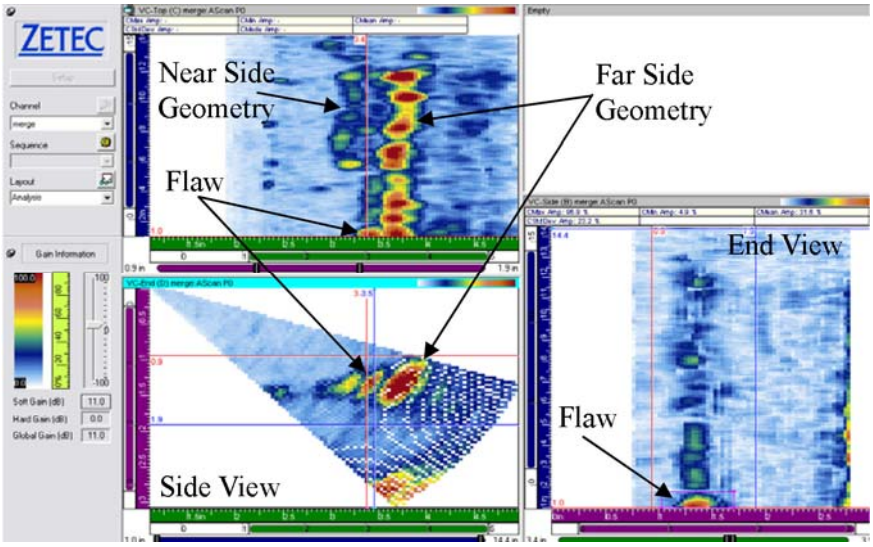


**Figure 4.8**. Data Images Showing a Flaw Signal Separated from Geometrical Indications

## 4.3 Discussion

The combined data indicate that near-side detection of IGSCC provides for a 71%–79% detection rate when using the applied phased array methods and scanning techniques. However, far-side detection rates drop significantly, with shear-wave detection from the far-side representing the lower extreme at 52%, as compared to the longitudinal wave detections at 68% or 69%. Earlier work (Anderson et al. 2006; Anderson et al. 2007) based on a machined-notch response showed that a longitudinal sound field passed through the weld with a minimal amplitude loss but exhibited significant sound field redirection. The shear-wave sound field (having a shorter wavelength) was severely attenuated (primarily by a scattering mechanism) by the weld material, but showed less redirection and beam skewing. At the frequencies typically applied, shear waves do not transmit through austenitic weld microstructures as efficiently as

longitudinal waves, therefore resulting in lower detection rates. Preliminary sound field mapping experiments at PNNL have also shown that the shear wave is broken up in passing through the austenitic weld material whereas the coherence of the longitudinal wave sound field is maintained.

PNNL was supplied with flaw true state information, so analyses are not representative of blind tests or field inspections. The investigation was focused on assessing current PA ultrasonic techniques for austenitic welds. In this regard, the detection results should be considered as a best-effort, given equipment and inspection conditions; that is, the arrays were not specifically optimized for the weld conditions and the weld crowns were not removed, which would have provided greater access for each of the PA modalities and probes applied. Because the true state location data were known for the flaws under examination, the results described here should not be considered representative of a blind test, only an assessment of state-of-art phased array capabilities to detect actual service-induced IGSCC. Typically, the detection process involved first identifying geometrical reflectors based on axial position and circumferential extent. A strong ID-geometrical signal that had a large circumferential extent provided a good reference point. The geometrical reflectors were then removed from further consideration and the remaining signals evaluated based on the true state knowledge. If an indication was present in the location of a known flaw and the signal was separable from other signals by amplitude or length for example, the indication was called a detected flaw. The data, whether from the near-side or the far-side, were generally cluttered with many signals to consider. The smaller footprint of the 2-MHz TRL probe provided better access to flaws and in some cases allowed the only access. Its sound field, however, was not as well focused or coherent as the 1.5-MHz TRL probe. Far-side detection rates were similar with both of these probes but it is believed that detection improvement would be obtained if the weld crowns were removed. This would ensure full insonification of the far-side area of interest. The results might then be augmented with a 1-MHz evaluation that would be less effected by attenuation, scattering, and beam skewing. At this lower frequency, the probe footprint would be larger so weld crown removal would likely be necessary for a meaningful inspection. The shear-wave inspection did not add value to the longitudinal-wave results of this study. While it is recognized that shear mode near-side inspections are an acceptable industry practice, this limited study did not show any improvement in the shear mode results (even on the near-side of the welds) as compared to the longitudinal mode results.

Signal discrimination could be improved by more effectively peaking of ultrasonic signals where weld crowns presently limit this function. More accurate specimen profiling in the critical weld area, presently not possible with the weld crowns in place, would also improve the data interpretation. It is also possible that flaw-tip signals could be detected in a linear or raster PA scan if closer access to the flaw could be achieved.

# 5.0 Summary and Conclusions

After initial studies at PNNL on the far-side inspection of machined flaws and implanted thermal fatigue cracks through austenitic stainless steel piping welds showed favorable results (Anderson et al. 2006; Anderson et al. 2007), PNNL was invited to examine specimens containing service-induced IGSCC at the EPRI NDE Center. Phased-array ultrasonic data were acquired on a series of specimens with three different probes and two different inspection modalities. The specimens were divided into two groups, a practice set and a secure set. Full access to the specimens was given for the practice set and the data were taken to PNNL for flaw detection analysis. During data analyses the flaw true state on these practice

specimens was known. The secure data were acquired with only outer-diameter (OD) access to the specimens. Secure data analyses took place at the EPRI NDE Center with a proctor in place to ensure specimen security. True state information was also provided for the secure data set.

The practice and secure data results were combined to maintain integrity of the secure set and showed that the TRL inspection and analysis produced a far-side detection rate of approximately 69%. The TRS results were lower at 52% and this data showed much more scattering of the beam in passing through the austenitic weld material. SNRs in both longitudinal and shear wave responses were good for detected flaw signals, suggesting that signal discrimination remains the most challenging aspect of flaw detection.

The 2-MHz TRL probe, while not producing as well-focused a beam as the 1.5-MHz TRL probe, had a smaller axial footprint allowing closer placement to the existing weld crowns, thus enabling more of the sound field to be projected into the far-side area of interest. This was an advantage in tight geometrical configurations. Lower frequency probes are less susceptible to beam steering, scattering, and attenuation, but the focal apertures are larger than higher frequency arrays with similar numbers of elements. This results in lower frequency probes having larger axial footprints, making weld crown removal necessary to improve far-side inspections.

Weld crown removal would also provide enhanced signal discrimination in two ways. The first is that in the absence of weld crowns, the inner diameter profile of the specimen in the complex weld region can be better determined. With a known profile, the mapping of ultrasonic flaw response signals to those of inside surface part geometry is greatly simplified, allowing the examiner to more readily eliminate geometrical responses in the complex data image. Secondly, more effective peaking of the ultrasonic signals can occur. This would likely be accomplished with raster scanning to peak both the corner and tip signals, when present. In summary, signal discrimination in this often complex inspection, and more specifically, complex data interpretation task, can be improved with weld crown removal in currently operating plants and should be considered in the event of new plant construction.

# 6.0 References

Anderson MT, SL Crawford, SE Cumblidge, AA Diaz and SR Doctor. 2007. "A Comparison of Ultrasonic Flaw Responses as Observed through Austenitic Stainless Steel Piping Welds." In *Proceedings of the Sixth International Conference on NDE in Relation to Structural Integrity for Nuclear and Pressurised Components*, EUR 23356 EN-2008, pp. 798-806. October 8–10, 2007, Budapest, Hungary. eds: M Bieth and J Whittle. European Communities.

Anderson MT, AA Diaz, SE Cumblidge and SR Doctor. 2006. "Capabilities of Ultrasonic Techniques for the Far-Side Examination of Austenitic Stainless Steel Piping Welds." In *Fifth International Conference on NDE in Relation to Structural Integrity for Nuclear and Pressurised Components*, May 10-12, 2006, San Diego, California. eds: M Bieth and J Whittle. European Commission Joint Research Centre.

# Appendix A

# Images and Detection Calls from Practice Data

# Appendix A

# Images and Detection Calls from Practice Data

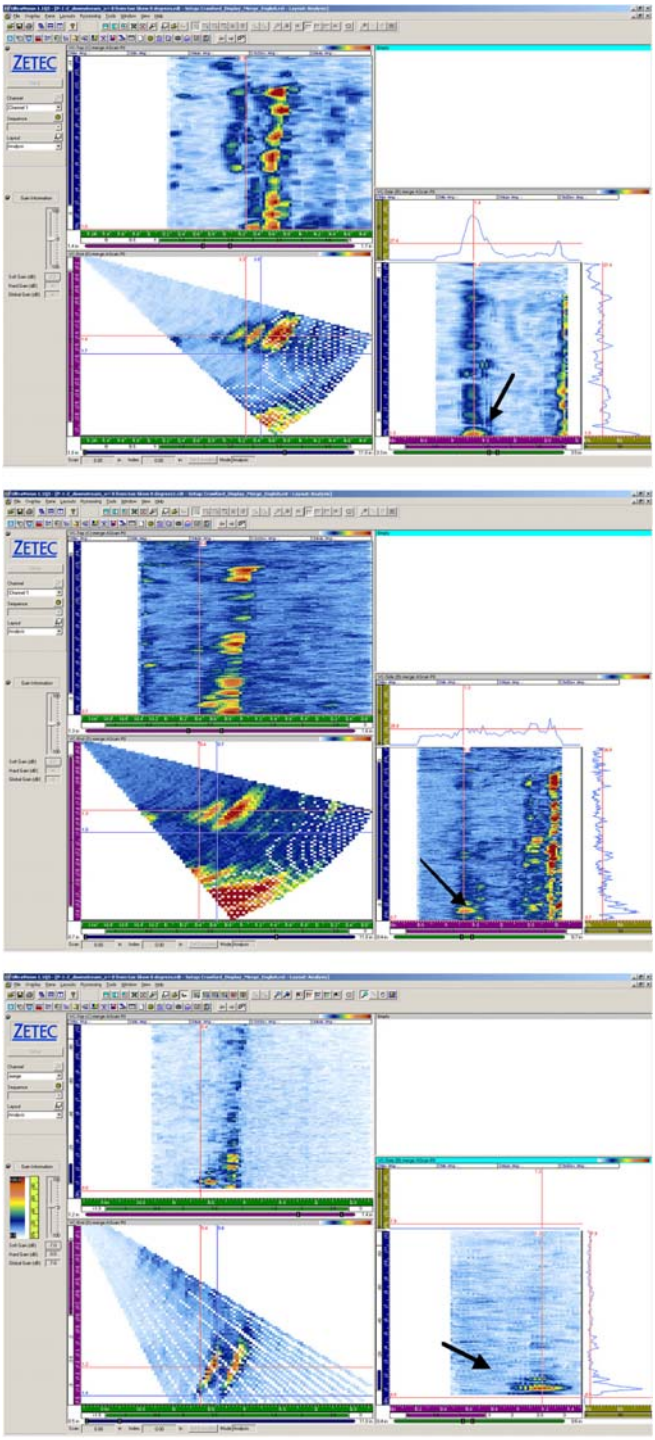


**Figure A.1**. P1-2 Downstream, Near Side with TRL 1.5 MHz, Mini-TRL 2 MHz, and TRS 2 MHz, Top to Bottom. Yes, Yes, Yes detected.

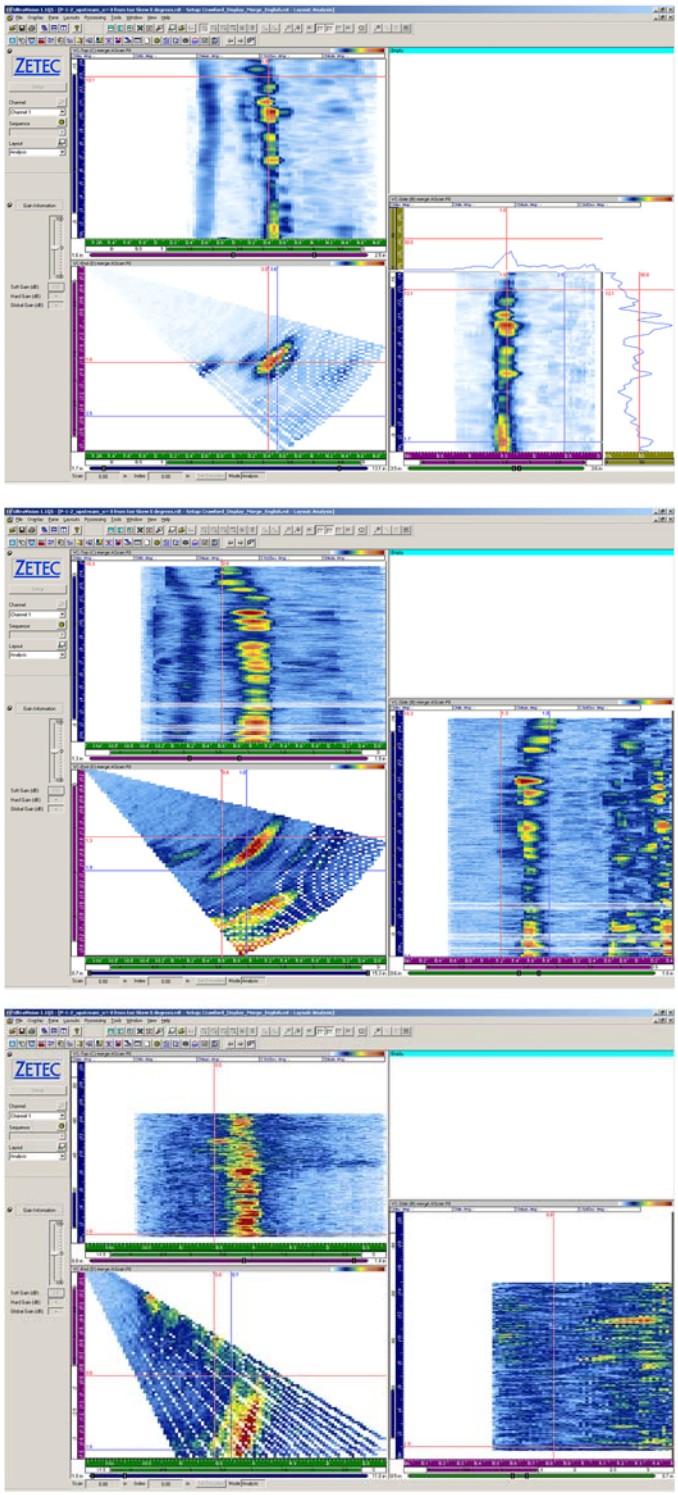

**Figure A.2**. P1-2 Upstream, Far Side with TRL 1.5-MHz, Mini-TRL 2-MHz, and TRS 2-MHz, Top to Bottom. No, No, No detected.

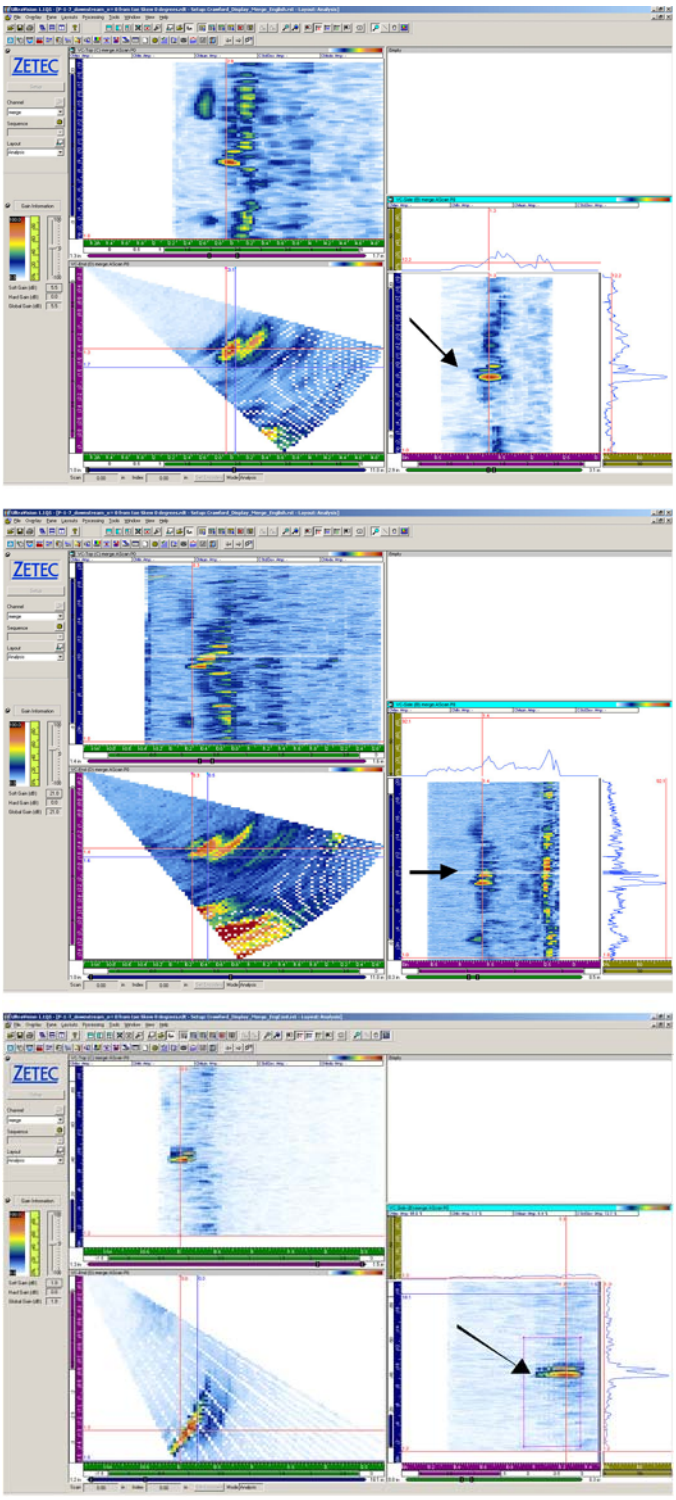

**Figure A.3**. P1-7 Downstream, Near Side with TRL 1.5-MHz, Mini-TRL 2-MHz, and TRS 2-MHz, Top to Bottom. Yes, Yes, Yes detected.

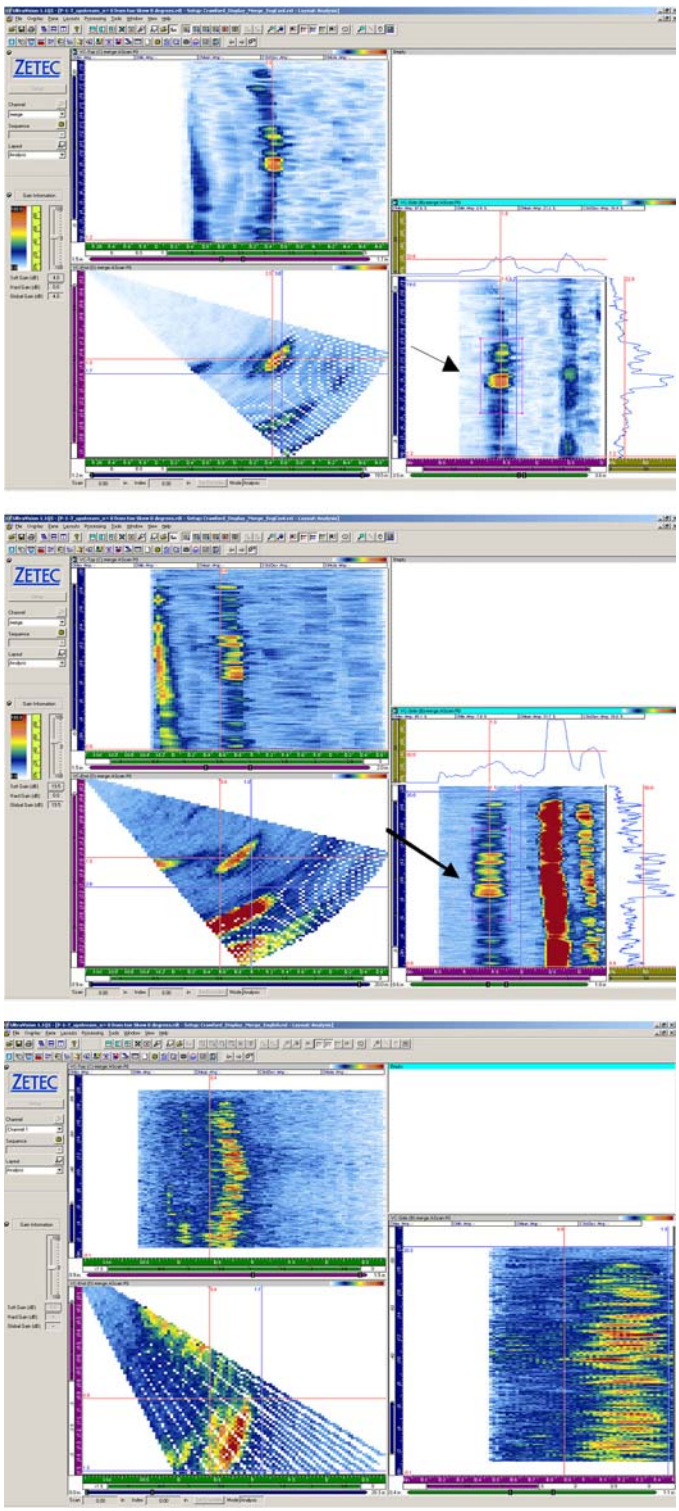

**Figure A.4**. P1-7 Upstream, Far Side with TRL 1.5-MHz, Mini-TRL 2-MHz, and TRS 2-MHz, Top to Bottom. Marginal, Marginal, No detected.

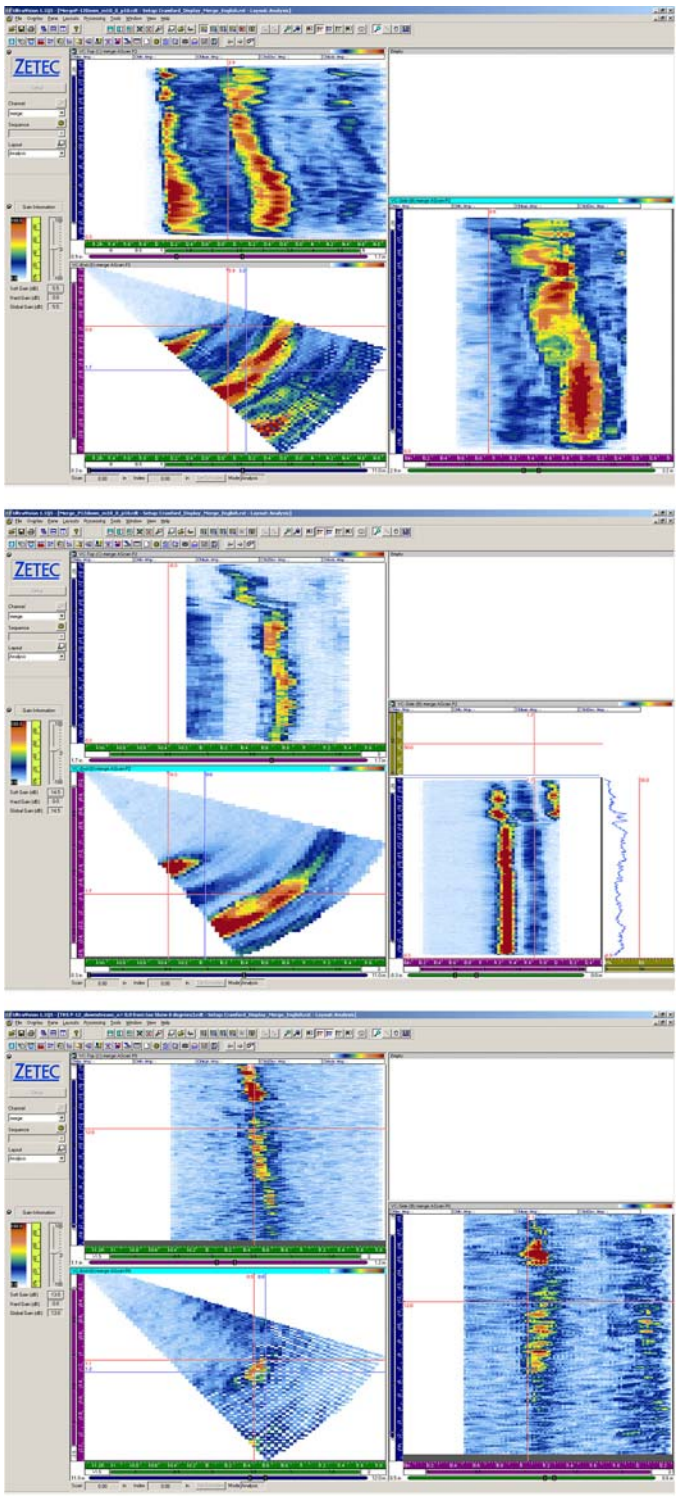


**Figure A.5**. P1-12 Downstream, Near Side with TRL 1.5-MHz, Mini-TRL 2-MHz, and TRS 2-MHz, Top to Bottom. No, No, No detected.

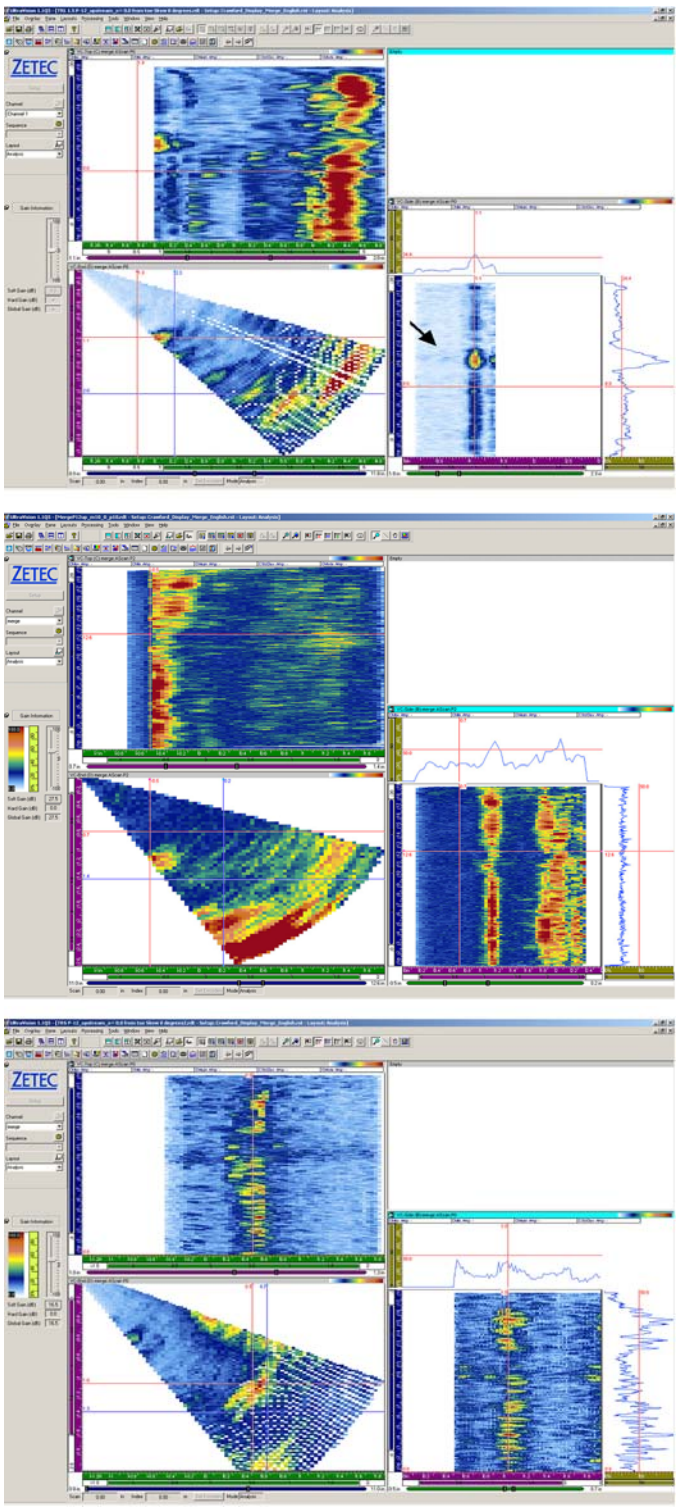

**Figure A.6**. P1-12 Upstream, Far Side with TRL 1.5-MHz, Mini-TRL 2-MHz, and TRS 2-MHz, Top to Bottom. Marginal, No, No detected.

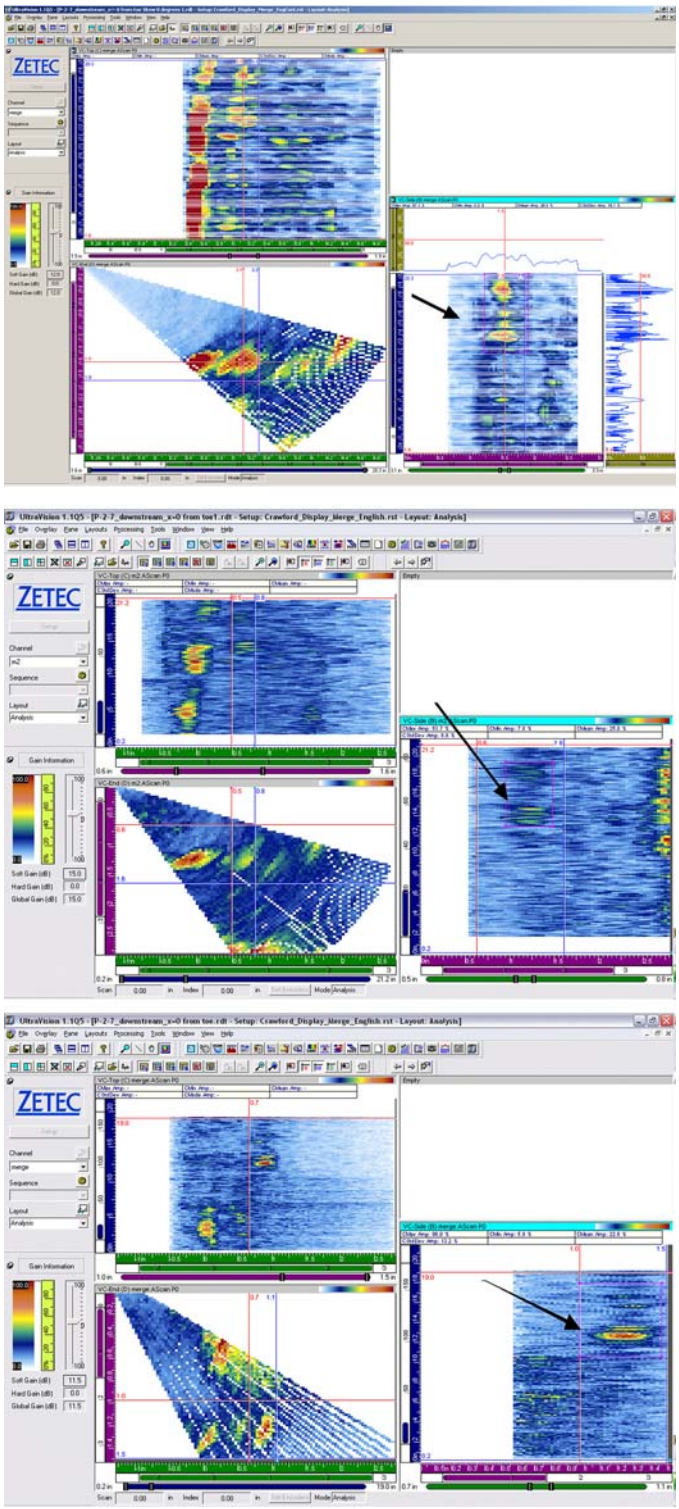

**Figure A.7**. P2-7 Downstream, Far Side with TRL 1.5-MHz, TRL 2-MHz, and TRS 2-MHz, Top to Bottom. Yes, Yes, Yes detected.

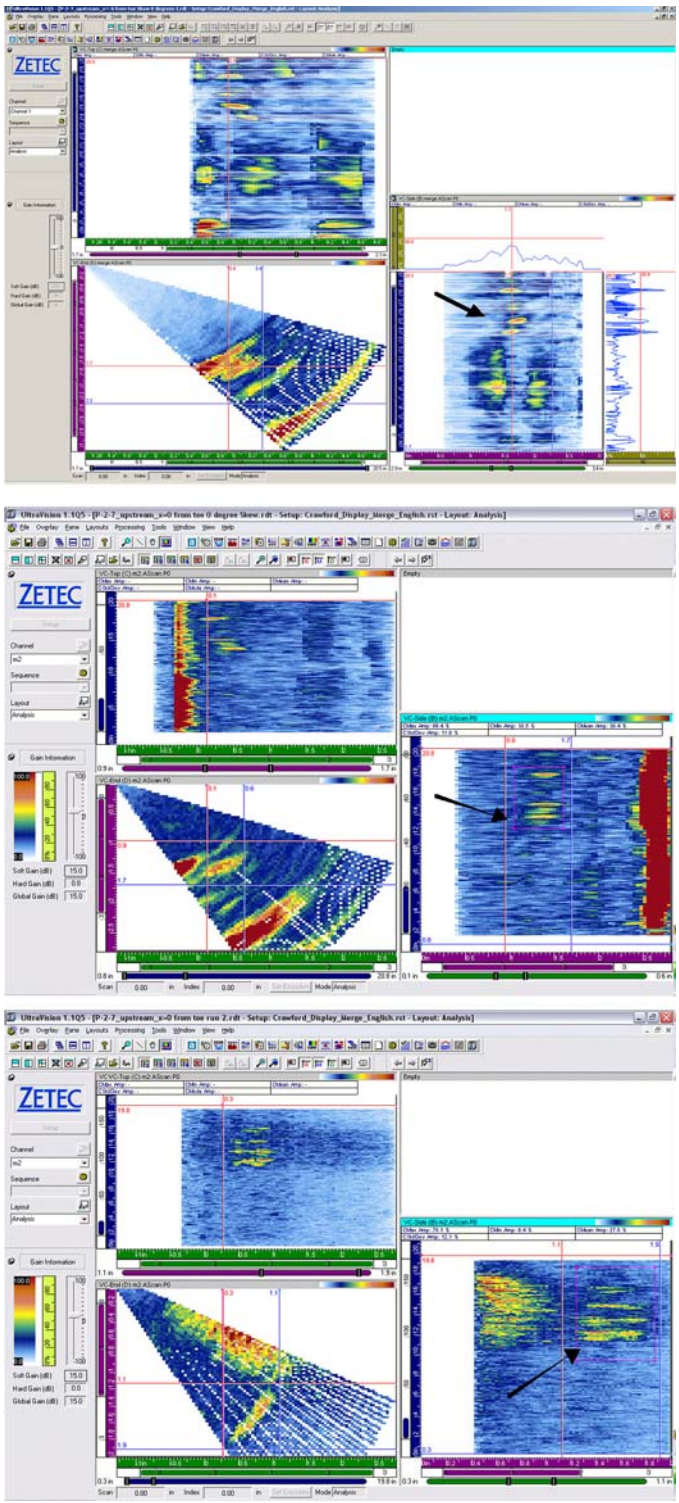


**Figure A.8**. P2-7 Upstream, Near Side with TRL 1.5-MHz, TRL 2-MHz, and TRS 2-MHz, Top to Bottom. Yes, Yes, Yes detected.

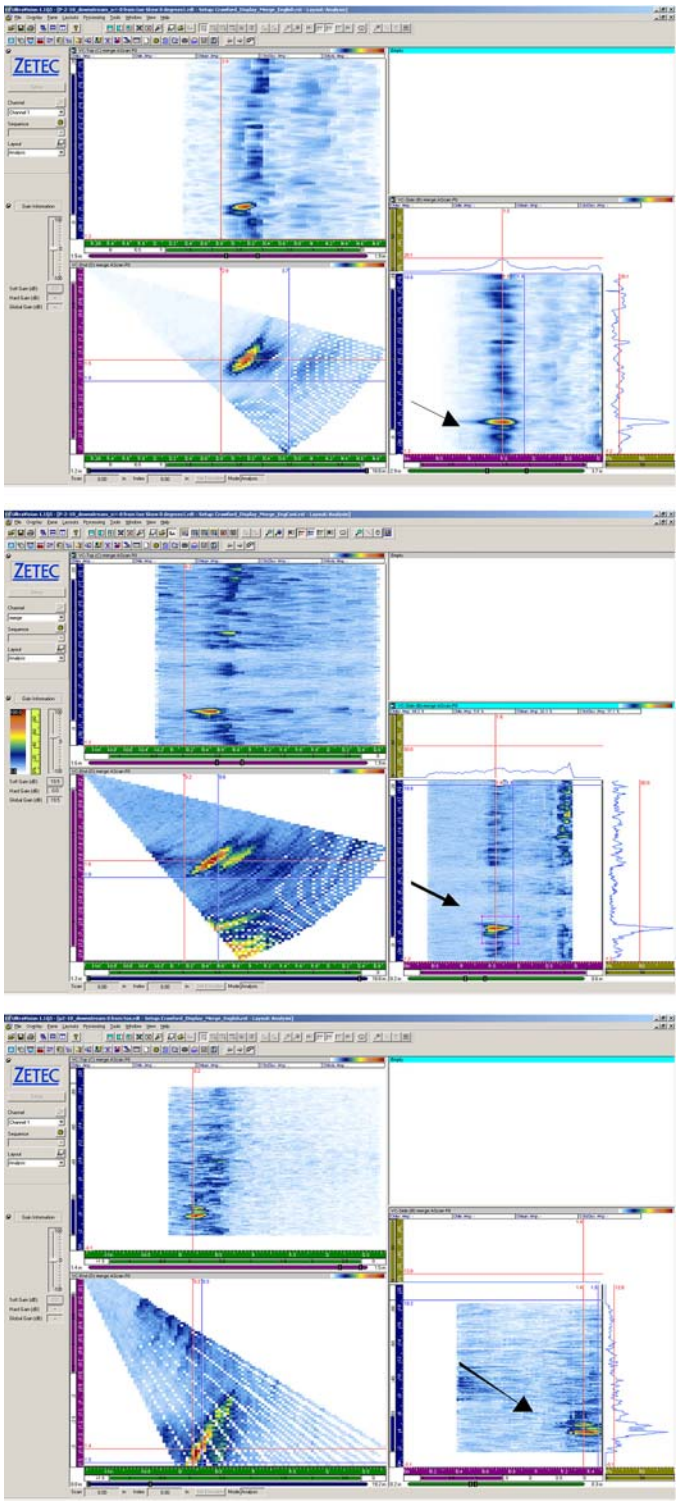

**Figure A.9**. P2-10 Downstream, Near Side with TRL 1.5-MHz, Mini-TRL 2-MHz, and TRS 2-MHz, Top to Bottom. Yes, Yes, Yes detected.

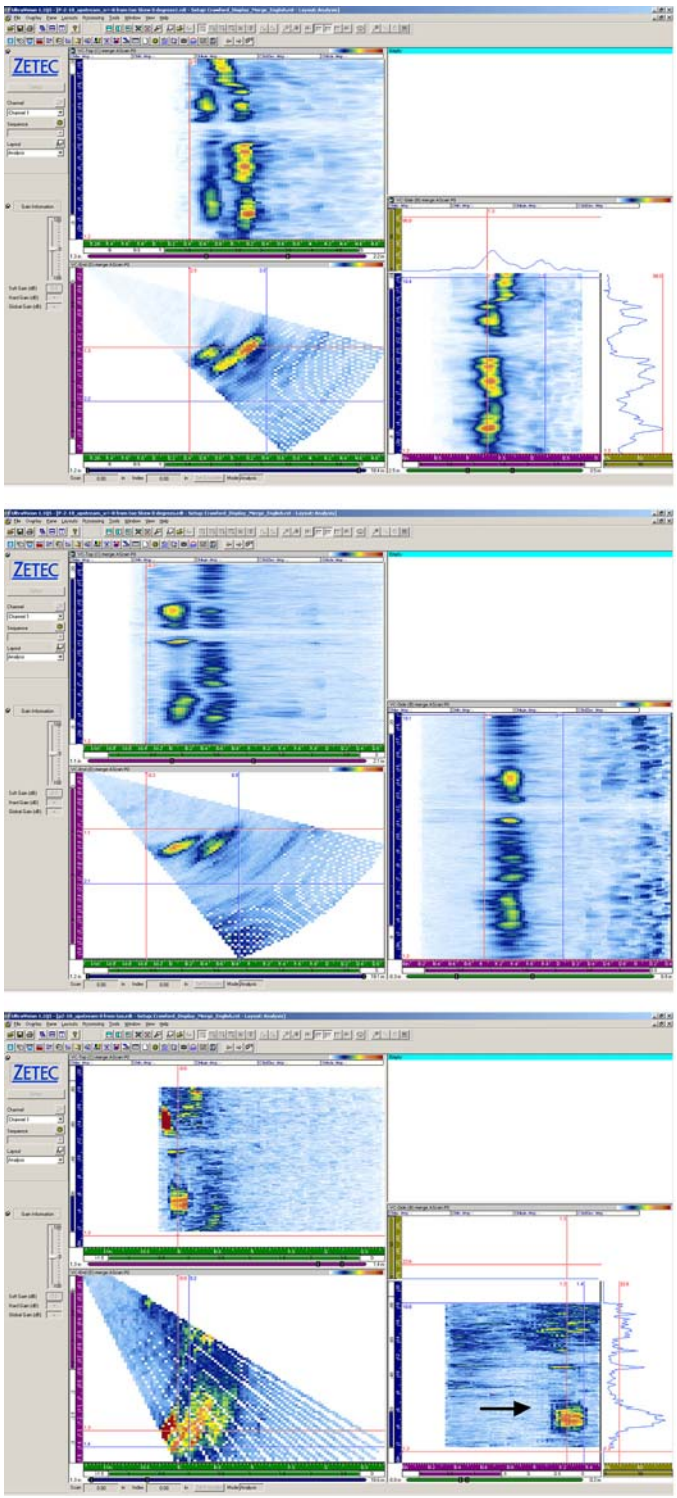


**Figure A.10**. P2-10 Upstream, Far Side with TRL 1.5-MHz, Mini-TRL 2-MHz, and TRS 2-MHz, Top to Bottom. No, No, Yes detected.

Pacific Northwest
NATIONAL LABORATORY

U.S. DEPARTMENT OF
ENERGY

902 Battelle Boulevard
P.O. Box 999
Richland, WA 99352
1-888-375-PNNL (7665)
www.pnl.gov